New pulsed jet using spark plasma discharge: Subsonic configuration

Benard, Nicolas; Zong, Haohua; Zhang, Yang; Kotsonis, Marios; Acher, Gwenael; Cattafesta, Louis N.; Bonnet, Jean-Paul; Moreau, Eric

DOI
10.2514/6.2020-2149

Publication date
2020

Document Version
Final published version

Published in
AIAA Scitech 2020 Forum

Citation (APA)
Benard, N., Zong, H., Zhang, Y., Kotsonis, M., Acher, G., Cattafesta, L. N., Bonnet, J.-P., & Moreau, E. (2020). New pulsed jet using spark plasma discharge: Subsonic configuration. In *AIAA Scitech 2020 Forum: 6-10 January 2020, Orlando, FL* Article AIAA 2020-2149 (AIAA Scitech 2020 Forum; Vol. 1 PartF). American Institute of Aeronautics and Astronautics Inc. (AIAA). https://doi.org/10.2514/6.2020-2149

AIAA SciTech Forum
6-10 January 2020, Orlando, FL
AIAA Scitech 2020 Forum

10.2514/6.2020-2149

New pulsed jet using spark plasma discharge: Subsonic configuration

N. Benard[1], H. Zong[2], Y. Zhang[3], M. Kotsonis[2], G. Acher[1], L.N. Cattafesta[3], J.P. Bonnet[1] and E. Moreau[1]

[1]*Institut PPRIME (CNRS UPR 3346, Université de Poitiers, ISAE-ENSMA), Futuroscope, France*
[2] *Faculty of Aerospace Engineering, Delft University of Technology, Delft, The Netherlands*
[3]*FCAAP, Florida State University, Tallahassee Florida, USA*

Active flow control is demanding for new actuation technologies as none of the actual available actuators has reached all the criterions for expecting an implementation in the coming years. Here, a new type of pulsed jet is designed and preliminary measurements of its performances in quiescent flow are conducted. Pulsed operation has been chosen because of the expected high efficiency of pulsed actuation in comparison to continuous blowing. The traditional pulsed jets being limited in term of frequency because of the use of a mechanical valve to achieve the desired pneumatic opening and closing of a jet provided by an external pressure source, the fast response of electrical discharge is exploited in the present investigation. The objective is to modulate the output of a small jet exhausting from a pressurized chamber. A spark discharge is used to affect the thermodynamic state of the gas in order to electrically achieve periodic cancellation of the chocked flow conditions at the throat upstream the jet exit. In the present study, such actuator with additional neck extension and jet diameter enlargement is investigated. The configuration results in a high-speed subsonic jet whose velocity amplitude is modified by an arc discharge with deposited energy from 18 to 780 mJ. Some characteristics of the jet are provided using optical methods such as high-speed Schlieren and PIV. In particular, it is shown that the jet flow velocity can be increased from 50 m.s^{-1} to 190 m.s^{-1}.

I. Introduction

In many high-speed flow conditions as encountered in full scale commercial or military aircrafts, active flow control requires actuators with specific characteristics. Particularly for high velocity flow control configurations (i.e., from high subsonic to supersonic regimes), high frequency and high authority actuators (in terms of flow speed or momentum) are required ([1], [2]). Some recent developments of active actuators for supersonic flow control can be found in Emerik *et al.* [3] and [4]. Pressurized flowing jets pulsed by mechanical valves have a high potential but they are limited in terms of frequency (up to typically a few hundred of Hz). Recently, the concept of synthetic jet using a spark discharge in a small cavity has been extensively developed with perspective of achieving high-frequency excitations. This actuator is usually referred as PSJA for Plasma Synthetic Jet Actuator. The concept has been initially proposed by Cybyk et al. [5], but recent advancements have been achieved as it was reviewed in Zong and Kotsonis [6]. This type of actuator is capable of producing a jet flow with high-velocity at high frequencies. For instance in [7], the authors have shown that high-velocity jet with a maximal velocity of about 300

[1] Nicolas Benard, Associate Professor, nicolas.benard@univ-poitiers.fr, AIAA senior member
H. Zong, Research assistant, H.Zong@tudelft.nl
Y. Zhang, Research faculty, yz12b@my.fsu.edu
M. Kotsonis, Associate Professor, M.Kotsonis@tudelft.nl
G. Acher, Post-doctoral researcher, gwenael.acher@univ-poitiers.fr
L.N. Cattafesta, University Eminent Scholar and Professor, lcattafesta@eng.famu.fsu.edu, AIAA associate fellow
J.P. Bonnet, Emeritus DR CNRS, jean-paul.bonnet@univ-poitiers.fr
E. Moreau, Full Professor, eric.moreau@univ-poitiers.fr

$m.s^{-1}$ can be obtained with high-frequency conditions (>5 kHz). The performances of PSJA are mainly related to the electrical parameters that control the plasma discharge regime but they also depend a lot on the geometry of the cavity. As discussed in [1], the transfer function of PSJA strongly depends on the geometrical parameters. In particular, accumulation of residual temperature in the cavity as well as insufficient refreshing period (suction period of the actuator cycle) are two factors limiting the repetition frequency of this type of actuator. The saturation frequency has been largely commented in [8], and it was concluded that when the repetition frequency is increased, the peak jet velocity can remain at a high amplitude but the jet duration time drops. It was theoretically demonstrated that the gas density in the cavity declines with increasing energy deposition and repetition frequency. During high-frequency actuation, the gas in the cavity does not recover the initial ambient pressure condition and thus the density in the cavity is slightly lower than the ambient density, which degrades the performance of the PSJA.

In the present investigation, we developed a new type of pulsed jet combining a cavity and a plasma discharge. However, as opposed to PSJA, the cavity is continuously supplied by a constant air pressure. Thus, this actuator results in a continuous jet that can be turned off by a mechanical valve. The objective here is to modulate the output of the jet from low to high-frequencies. The basic principle is to increase the temperature at a sonic throat located upstream of the jet exit with the help of a spark discharge (Fig. 1). For an ideal gas, the flow rate being proportional to the inverse of the square root of the temperature at a constant settling chamber pressure, the jet flow rate can be varied. Although it also uses a plasma discharge, the present method is then quite different from the PSJA as the proposed device uses extra air for thermal balance. Because of the addition of an extra source of pressure to fill the cavity, it is expected that this device could achieve high-frequency forcing without degrading the mean and time-resolved performances.

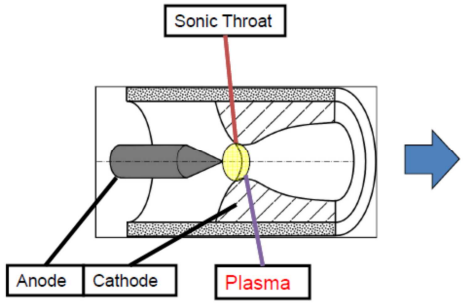

Figure 1: Schematic of the plasma-assisted pulsed jet actuator.

II. Description of the plasma-assisted pulsed jet

A. Actuator design

The plasma–assisted pulsed jet is composed of a pressurized chamber, in which the pressure is controlled and remains constant at a given value (typically 1.4 bar differential in the present investigation), a sonic throat just in front of the device exit and a thin conductive needle centered within the cavity. The needle is made of tungsten, its length is 2 cm and its radius of 800 μm ended by a 15° tip cone. However, the effective volume is reduced to 125 cm^3 due to the presence of the needle and its support.. The support of the needle can be translated in order to adjust the distance between the end tip of the needle and the jet exit. Here this distance is kept constant at 2 mm but it can be varied as a future parameter to optimize. The exit of the system is made of a 1-mm diameter hole with a length of 3 mm. The exit hole of the model is located at the center of a circular insert with a diameter of 16 mm. This insert is mounted to the aluminum output support. It is made of tungsten,to reduce erosion, which can potentially cause possible geometric modification of the output hole during the different tests. In the standard operation, this geometry produces an initially sonic jet. Presently, an aluminum extension is fitted at the end of the actuator. This neck extension has a circular orifice whose diameter is 3 mm and length of 17 mm. This extension is perfectly aligned with the hole forming the sonic throat. In such a configuration, the jet exhausting from the device evolves from sonic to subsonic regime due to the sudden expansion from 1 to 3 mm (with feeding pressure of 2.4 bar, i.e. 35 psi). The

shop air is connected to the back of the model, and an additional supply line can be used to fill the cavity with seeding particles for optical flow measurement such as PIV.

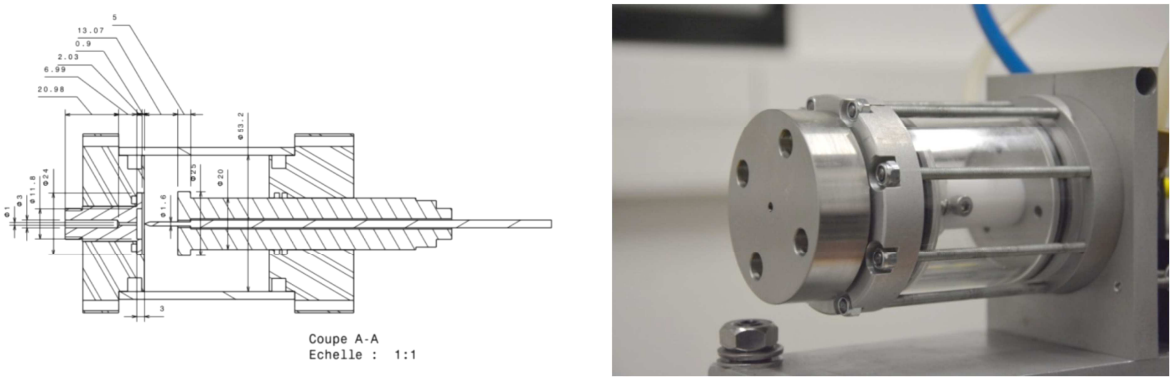

Figure 2: Technical drawing of the initial model and image of the plasma-assisted jet in subsonic (long neck extension) configurations

B. Electrical setup

The primary principle of this device is based on the introduction of thermal energy deposition at the sonic throat using an arc discharge. Here, the anode electrode is the needle inside the cavity while the grounded electrode is the insert piece made of tungsten. The power supply used to produce the spark is strictly similar to the one used by Zong and Kotsonis [8] for PSJA. A discharge power supply combining high-voltage trigger pulse and capacitive discharge is used as shown in Figure 3. The ionization of the 2-mm inter-electrode gap is caused by low-energy trigger pulses that are delivered by a high-voltage amplifier (Trek 30/20). These pulses have amplitude of 12 kV and a pulse width of 80 µs. In the present investigation, only single-shot mode is investigated so the repetitive frequency of the pulses is fixed at 2 Hz. When the gas is ionized, the high-voltage amplifier cannot provide sufficient current and the voltage of the pulse suddenly drops. Placed in parallel to the electrical circuit producing the trigger pulses, a capacitive discharge provides the energy to locally increase the temperature at the sonic throat. A capacitor charging power supply (peak voltage 2.5 kV, power 2000 W) is used for charging the capacitor C1 (capacitance 1 µF, withstanding voltage 5 kV). As soon as the inter-electrode gap becomes conductive due to the ionized channel, the energy stored in capacitor C1 is released rapidly into the actuator cavity via arc heating. The capacitor C1 is periodically recharged to maintain a constant repetitive frequency over time. The electrical circuit also includes a high-voltage resistor R1 (resistance 1 kΩ, power 200 W), whose purpose is to limit the charging current as well as high-voltage diodes for protecting the DC and pulsed power supplies. As shown by Zong [8], the additional high-voltage trigger pulse has the advantage of simplifying the system without the use of a third electrode as a trigger source, and it also fixed in time the ignition of the spark discharge while reducing the EMI. However, a variation of about ±10µs in the ignition time of the ionization channel has been observed.

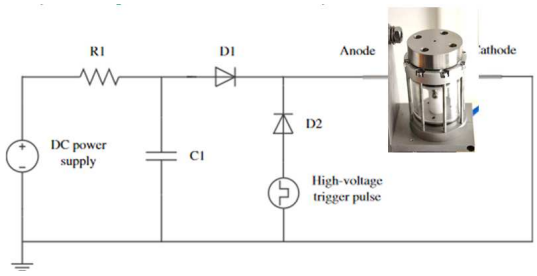

Figure 3: Electrical circuit used to power the plasma-assisted pulsed jet

C. Measurement setup

Electrical measurements of the discharge have been conducted. High-voltage probes (Northstar PVM-1) are used to monitor the voltages produced by the trigger pulse as well as the voltage at the anode electrode. A current transformer (Stangenes model 0.5-0.01) is used to monitor the current passing through the arc discharge. These probes are connected to a high-resolution (12 bits) oscilloscope with 500 MHz bandwidth (Lecroy HDO 4054A). All signals are recorded with 10 Ms/s in order to achieve a sufficient time resolution in view of recording properly the fast voltage drop and current increase when the medium becomes conductive and the capacitor C1 discharges.

The plasma-assisted pulsed jet principle is based on modification of the jet velocity by sudden changes in temperature imposed by an arc discharge. The arc is localized in the actuator but the thermal is convected in the fluid medium because of the differential pressure imposed in the cavity chamber. Then, the spatial and temporal changes of the refractive index *n* of air can be easily detected by using a Schlieren system [9]. Here, a linear Schlieren is used (see Figure 4) where a small bright LED source illumination, propagating in the z-direction, is collimated by a 300 mm focal lens and then focused by a second spherical lens of similar focal (f/4). The LED (CBT 120) light source is driven by an electrical circuit inspired from Buchmann *et al.* [10] where a high-current (210 A) is forced on the LED for a short period of time. The major challenge here is caused by the need for a short duration illumination (1 µs) to freeze the flow while a high-repetition rate (from 100 to 150 kHz) is also required to image the flow in a time-resolved manner. This system makes non-steady waves and flow turbulence visible but at the price of a low brightness of the images. An horizontal sharp razor blade is placed at the light focus to record the refractive-index gradient $\partial n/\partial y$. A high-speed CCD camera (Phantom V2012) equipped with 180 mm objective (Tamron 180 mm F/3.5) and 1.4× teleconverter is used to image the flow. In order to reach high-repetition rate, the sensor of the camera is cropped to a reduced field of view of 984×386 for 100 kHz acquisitions and of 600×386 for 150 kHz measurements. Here, phase-locking the schlieren images to the actuator control signal is complicated by the jitter in the ignition of the arc discharge (this will be discussed later in the paper), so only time-resolved Schlieren measurements are conducted. This non-intrusive technique is expected to provide observation of transient perturbation caused by the thermal deposition that will cause a shift in the refractive index of the subsonic jet.

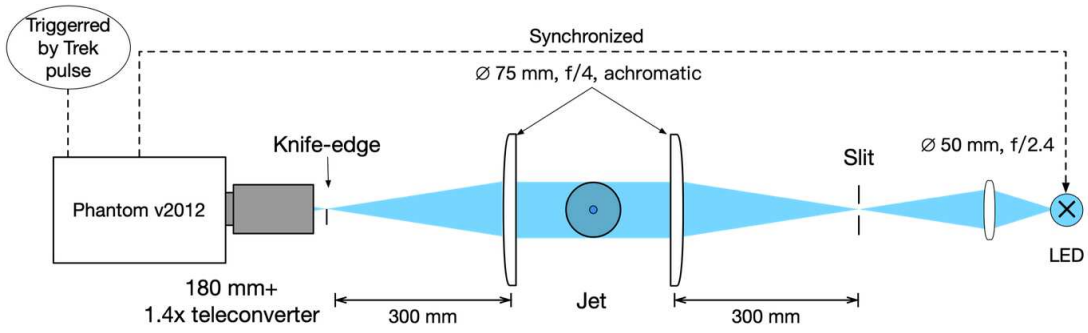

Figure 4: Sketch of the Schlieren system used to image the jet perturbed by the arc discharge.

Fluid flow measurements have been performed using a low-speed 2D2C PIV system. This type of measurement is highly challenging as it combines a small size jet flow with high-speed regime. Here, a dual pulsed laser (Evergreen 70-200 mJ at 532 nm) delivering up to 100 mJ at 15 Hz is used to produce the laser sheet. The optical system in front of the laser source has been optimized to finally obtain a laser sheet with a thickness of 500 µm which is measured by a photodiode. This laser sheet crosses the jet in its central location. A high-resolution PIV camera (Imager pro X) is used with a focal double adapter and a 200 mm Nikor objective. The seeding particles are injected directly inside the cavity of the actuator while maintaining the cavity pressure to 1.4 bars by adjusting the external compressed air. Phase measurements are preferred here in order to detail the dynamic of the subsonic jet when an electrical energy deposition is superimposed on the natural jet. The PIV system and the command signal of the actuator are synchronized by a PTU and the repetition rate of acquisition is set to 2 Hz. During the experiment,

the opening time of the CCD camera and voltage at the anode electrode are simultaneously monitored. The time delay between the opening of the camera and the capacitor discharge is automatically determined and values are saved instantaneously in an external text file using a digital oscilloscope (Lecroy 4054). A total of 9 phases with 500 image pairs for each case are recorded. For each acquisition in one phase, the time delay between the arc discharge and the PIV acquisition is known and this information can be exploited after experiment using the recorded text file. The final field of view is 18×10 mm². Images are separated by a typical time delay of about 1.5 μs and each of the image pairs are processed using multi-pass correlation algorithm using Davis Lavision 8.4 software. The final pass of the multi-pass algorithm is set to 16×16 interrogation windows with 50% overlap, the final resolution of the PIV measurements is one vector every 120 μm.

III. Results

A. Electrical measurements

The electrical characteristics are investigated first. As it is shown in Figure 5, the plasma discharge between the needle and the cathode is strongly affected by the static pressure in the chamber. In absence of differential pressure (ΔP=0 bar), the spark discharge is limited to the inter-electrode gap (Fig. 5a). In case of a differential pressure of 1.4 bars, the plasma initiates at the tip of the needle but it is elongated beyond the grounded plate (see Fig 5b where the plasma plume is shown in absence of the 17 mm extension). Consequently, a strong modification of the electrical characteristics is expected depending on the pressure settled in the chamber. However, this parameter will not be discussed in detail here.

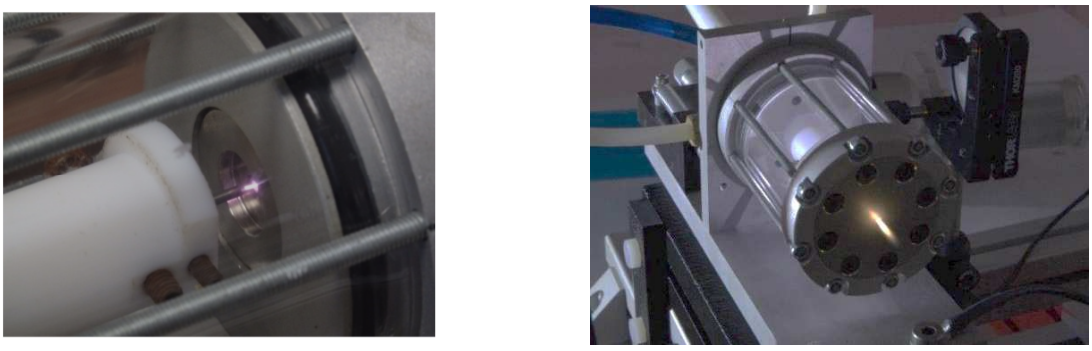

(a) (b)

Figure 5: Image of the plasma-assisted pulsed jet in operation with supplying air pressure of (a) 0 bar and (b) 1.4 bars.

The case of zero differential pressure (Δp=0) is shown in Figure 6, with the capacitor charging power supply being set to dc voltages from 250V to 1250V. Before the TTL signal used to ignite the spark, the voltage is maintained at a constant value supplied by the capacitor charging power supply. The opening of the AC source leads to an increase of the voltage up to the pre-ionization of the gas in the inter-electrode gap. In the present geometrical conditions, the pre-ionization is obtained for a voltage level of 2.2 kV, resulting in a glow discharge forming from the needle to the cathode. This ionized region is conductive, and then the capacitor C1 suddenly and abruptly discharges within 200 ns while the current starts to increase until it's limited by the rest of the electrical system. By increasing the capacitor charging voltage from 250V to 1250V, the current passing through the electrical arc can be increased from 18 to 95 A.

As illustrated by Figure 4, the pressure in the chamber strongly modifies the duration of the electrical arc. Thus, electrical measurements have also been performed in the case of a differential pressure of 1.4 bars. The results for two values of dc charging are shown in Figure 7, the results obtained at Δp=0 being also plotted for comparison. The pressure level in the chamber makes the pre-ionization step more unstable. Indeed, here the voltage threshold causing the gas in the inter-electrode gap to partially ionize and begin to be conducting varies between 3.2 and 4 kV.

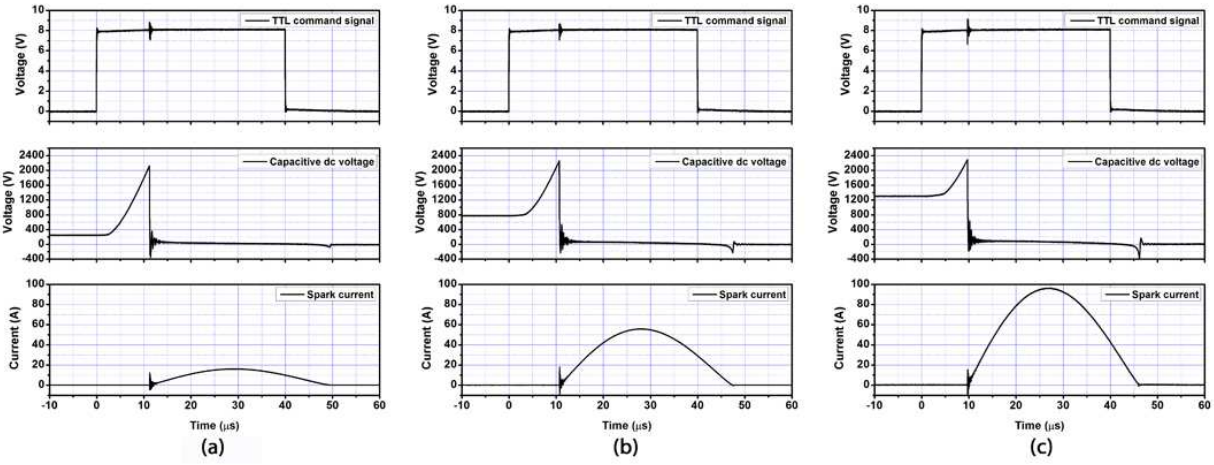

Figure 6: Typical traces of the signal command, voltage at the needle tip and current passing through the plasma discharge for the plasma-assisted jet powered by dc voltages of (a) 250V, (b) 750V and (c) 1250V. Differential pressure set to Δp=0.

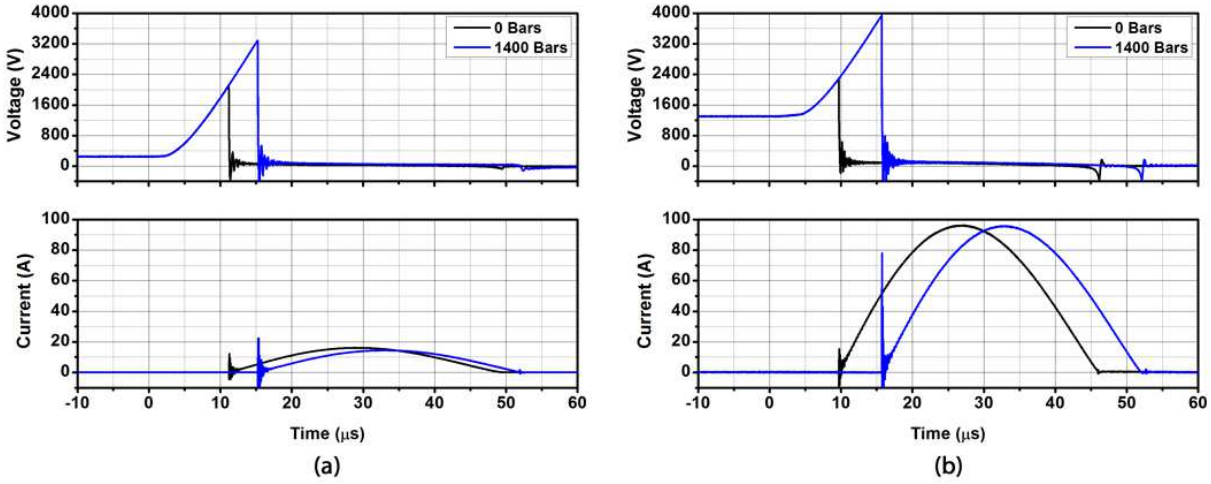

Figure 7: Typical traces of the voltage at the needle tip and current passing through the electrical arc for C1 capacitor charged at (a) 250V, and (b) 1250V. Differential pressure set to Δp=0 and Δp=1.4 bars.

By recording with high-temporal and high dynamic the voltage drop when the capacitor is discharged, the energy deposition produced by the arc can be computed (Figure 8). This energy deposition can be easily adjusted by modifying the charge of the capacitor C1. For a capacitor charging voltage between 250V and 1250V the deposited energy can reach 450 mJ if no differential pressure is applied in the chamber. With pressurized air inside the cavity, the energy deposition can be significantly increased. At Δp=1.4 bar, the maximum energy deposition reaches 780 mJ indicating a 74% maximum increase in the energy deposited at the nozzle throat.

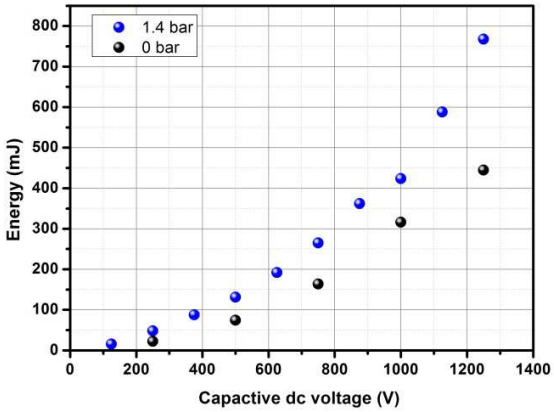

Figure 8: Energy per pulse delivered into the plasma-assisted jet vs dc voltage used to charge the capacitor

B. Observations by time-resolved Schlieren

Results of the time-resolved Schlieren operated at 100 kHz are shown in Figure 9 for instantaneous Schlieren images from t=0 μs to t=450 μs. Here, the energy deposition of the arc discharge is 48 mJ. The image at t=0 μs illustrates the jet flow before the generation of the arc discharge and thus corresponds to a natural flow configuration (continuous jet mode). The jet being fully subsonic and the jet temperature equal to the room temperature, no significant density gradient can be observed at this time because of a lack of sensitivity of the Schlieren system in such a condition. At t=30 μs, the arc discharge has been formed inside the cavity and a hot jet starts to be convected in the field of view. A vortex ring is formed in front of the jet with two opposite cores being clearly visualized. Several compression waves propagating in the field are also observed and travelled in the field of view at high-speed (propagation speed about 380 $m.s^{-1}$ based on grey-scale levels). It is not clear if these shock waves originate directly from the sudden change in pressure caused by the arc discharge or if they correspond to a signature of multiple shock wave reflections inside the 17-mm neck extension. From time t=60 μs to t=120 μs, the density gradient is largely increased because of the hot gas exhausting from the cavity, and the gradual increase of the front vortex ring can be observed. As it was reported for PSJA [11], at a certain time (here t=120 μs) the front vortex ring evolves into a spherical vortex. One can notice that up to time t=180 μs the jet flow presents two distinct regions whose are differentiated by the intensity of the density spatial gradient. The brighter region is seen in the first instants of the perturbed jet and the mean propagation speed of its core is about 120 m/s. This region is followed by a darker one corresponding to a hot jet with low density that propagates at lower speed (70 m/s). This hot jet reaches the end of the field of view within t=420 μs and it exhibits a gradual propagation speed reduction as well as a gradual heat diffusion leading to a signature becoming brighter with time.

In a second series of Schlieren, the field of view has been reduced in order to increase the repetition rate of the system to 150 kHz. The magnitude of the deposited energy has been varied from 48 mJ to 88 mJ. These data (not shown here) can be used to estimate the instantaneous propagation speed of the high-density air exhausted from the cavity in the first instants ($t \leq 66$ μs) after the arc discharge by grey-level analysis. The results are summarized in Figure 10. The front jet attains a maximal propagation speed at time t=40 μs while its front jet speed reduced later. By increasing the deposited energy, a higher peak propagation speed is recordes (increase by 15%).

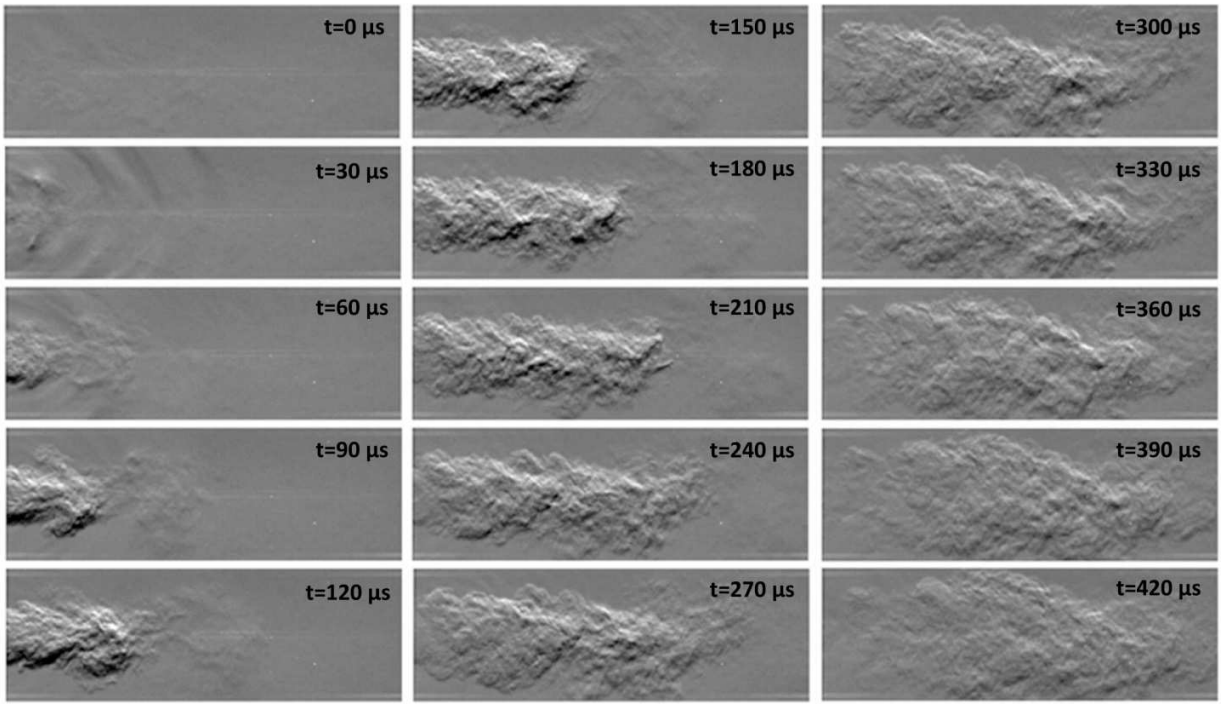

Figure 9: Time evolution of the 3-mm jet perturbed by a single arc discharge depositing 48 mJ at the internal jet throat. Exposure time of 1 µs.

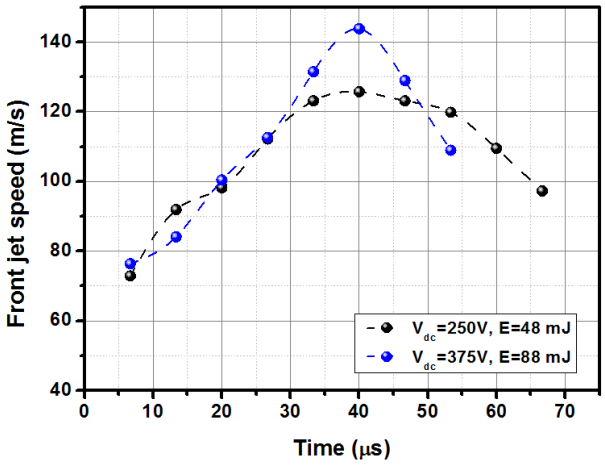

Figure 10: Front jet propagation speed of the high-density air expelled from the cavity in the first instants.

C. Fluid flow measurements by PIV

C-1 Time-averaged characteristics of the jet flow without discharge

The flow field in case of air pressure set to 1.4 bars differential in the cavity and without arc discharge is shown in Figure 11a (continuous jet mode). The jet formed at the exhaust of the plasma-assisted pulsed jet presents a jet core velocity of about 50 $m.s^{-1}$. Its potential core length is significantly short with a maximum velocity maintained only in

the first 1.2D (Figure 11b). Indeed, the virtual origin of the jet is inside the neck extension. By considering the total length of the neck, the potential core length is then of about 6.9D. The velocity along the *y* direction corresponds to top-hat profiles (Figure 11c) whose half-width increases linearly with distance *x* while the centerline velocity decays with a quasi linear trend. If the jet is considered as perfectly axisymmetric, the mass flow rate is of 0.6 g/s in the initial region (i.e., before surrounding fluid entrainment).

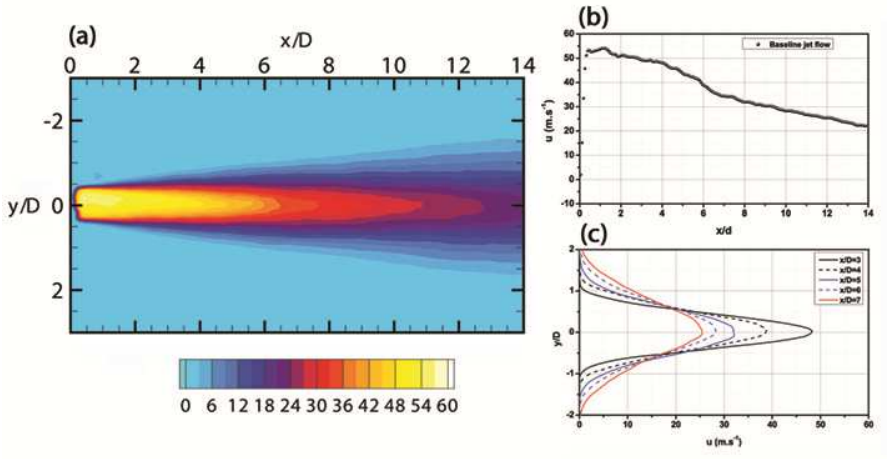

Figure 11: Time-average flow field (a) without spark discharge, (b) centerline jet mean velocity and (c) y velocity profiles at several x/D locations.

C-2 Procedure for data selection

The objective of the pulsed jet assisted by plasma is to modulate the output velocity of the jet to convert a continuous jet into a pulsed one. Consequently it is of primary importance to characterize the dynamic of the jet flow in presence of the spark discharge, and then the analysis of the time-averaged flow field only has minor interest. As it was described in the experimental setup, the PIV measurements have been conducted for 9 phases, or more precisely for 9 time delay between the signal command at the origin of the trigger pulse and the opening of the CCD camera shutter. The use of a trigger pulse to pre-ionize the gas is helpful in regularizing the ignition of the capacitor discharging however the technic is still perfectible. An illustration of different jet flow seeded by the PIV particles is shown in Figure 12 for a time delay imposed at 125 µs. The capacitor is charged with 750V resulting in an energy deposition of 266 mJ. One primary visible effect of the arc discharge is the production of two counter-rotating structures as they were observed in front of the jet by Schlieren. Figure 12 illustrates perfectly the difficulty to perform accurate phase measurements because of the jitter in the ignition of the capacitive discharge. It is clear that the vortex rings are located at different *x* locations in each of the selected images when they should be perfectly at a same *x* location if there was no jitter. It can be concluded that averaging all the 500 images recorded at a specific time delay without considering possible jitter will drastically affect the convergence of the resulting flow field and the quality of the phase reconstruction.

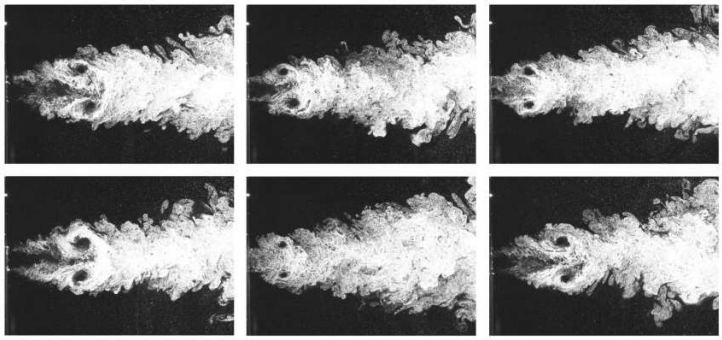

Figure 12: Illustration of the seeded flow at a constant time delay of 125 µs.

To anticipate this issue and in order to propose an offline solution, a time stamp is affected at each instantaneous flow field thanks to the time delays automatically recorded between the capacitor discharge and the opening of the camera. An illustration of the recorded time delay between the camera and the arc formation is shown in Figure 13a for an imposed phase delay of 85 µs. In fact, only about 65 instantaneous flow fields correspond to the imposed delay. By considering an acceptable jitter of 4 µs (i.e. a spatial displacement of 200 µm), the time-average can be computed based on 170 realizations. However, the time jitter is not the only contributor that may affect the quality of the averaging process. Indeed, the arc discharge is systematically formed at the needle tip but it does not always reach the grounded region at a same location. Furthermore, the energy deposition can suffer from slight fluctuations cycle to cycle (see the different velocity fields in Figure 13b where the real time delay is equal to 86±0.2µs). As a result a second selection is done on the velocity fields before computing the phase average. Each velocity field is spatially correlated with all the vector fields whose real time delay is in the range selected previously (imposed time delay ±2 µs) and all correlation coefficients are recorded. The case with the maximum number of cross-correlation coefficients above a threshold value of 0.85 is identified, and the corresponding images are used to calculate the time average at a given phase time.

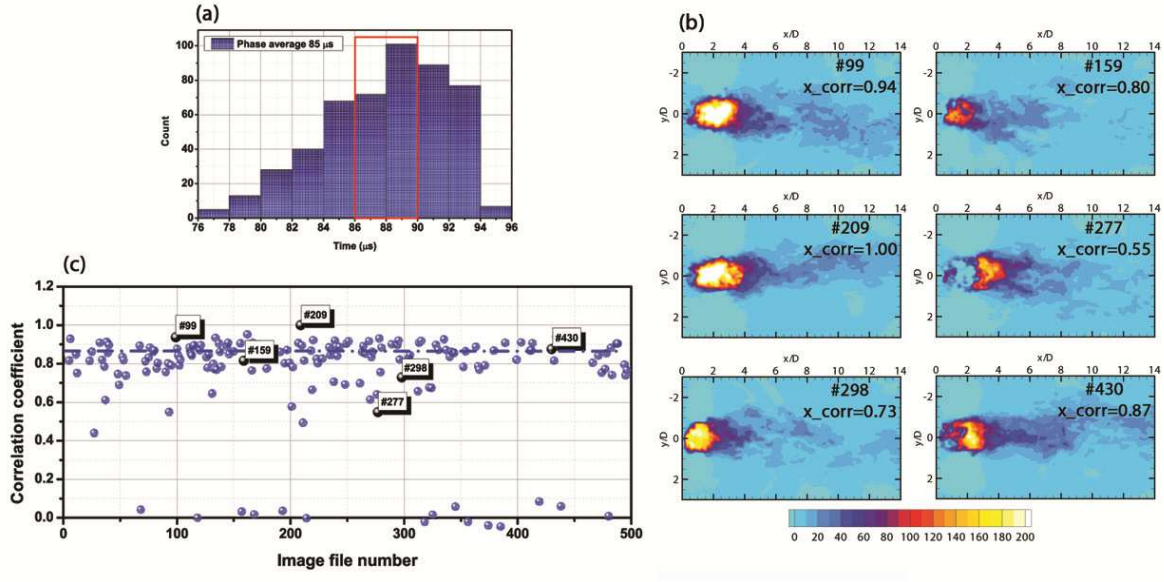

Figure 13: (a) Distribution of real time delays, (b) six instantaneous flow fields at a same real time delay of 86 µs, and (c) spatial correlation coefficient in the series of 500 instantaneous. All figures correspond to an acquisition delay imposed at 85 µs

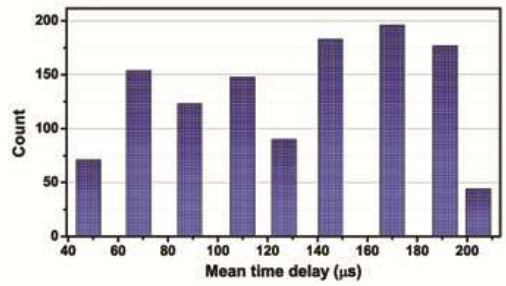

Figure 14: Numbers of vector fields used to compute the time-average at a given mean time delay

C-3 Phase-averaged results

The phase-averaged flow fields are presented in Figure 15. The capacitor is charged with a dc voltage of 750V, the resulting energy deposition is then 266 mJ per pulse. The two velocity components (u_x and u_y), velocity vectors and streamlines plots are all proposed in the figure where each phase is separated by 45±0.5 μs. The velocity field corresponds to a jet flow similar to the one without arc discharge is combined with a high-speed region in the central region of the jet. As for PSJA, the energy deposition at the exit orifice of the cavity is responsible for the formation of a high-speed jet flow but here this secondary jet is superimposed on the natural one. The jet velocity is never zero and it presents strong oscillations in its peak value as it was anticipated from the actuator principle. The velocity in the high-speed region caused by the arc discharge is not constant. A peak value of about 190 $m.s^{-1}$ is observed in the phase delay equal to 85 μs. Because of entrainment between the high-speed core and surrounding quiescent fluid, the high-speed region is surrounded by two strong contra-rotating vortices that can locally contract the core of the jet. These structures can be associated with the front vortex ring observed on the images get by Schlieren technique. The observed peak velocity is higher than the one measured by Schlieren but the energy deposition is also considerably higher. The peak velocity at different time delays after the arc ignition has been extracted and plotted in Figure 15. The peak velocity (about 190 $m.s^{-1}$) is attained 90 μs after the arc formation. This maximum speed is observed over a short period of time (from 90 to 110 μs) while a velocity decay is reported in the following 90 μs. In the final phase obtained during the PIV experiment, the high-speed core has a velocity of 120 $m.s^{-1}$, a value still significantly higher than the velocity of the nominal jet (50 $m.s^{-1}$). These results confirm a strong modulation of the jet speed by using an electric driven thermal perturbation. The modulation of the air jet ejection velocity corresponds here to a velocity increased by 280%. The tests performed do not provide a reliable basis for determining the modulation rate in terms of mass flow rate. However, there is no doubt that such a high level of perturbation (fluidic or even simply thermal) will have an effect on a flow, whether in tangential or transverse conditions.

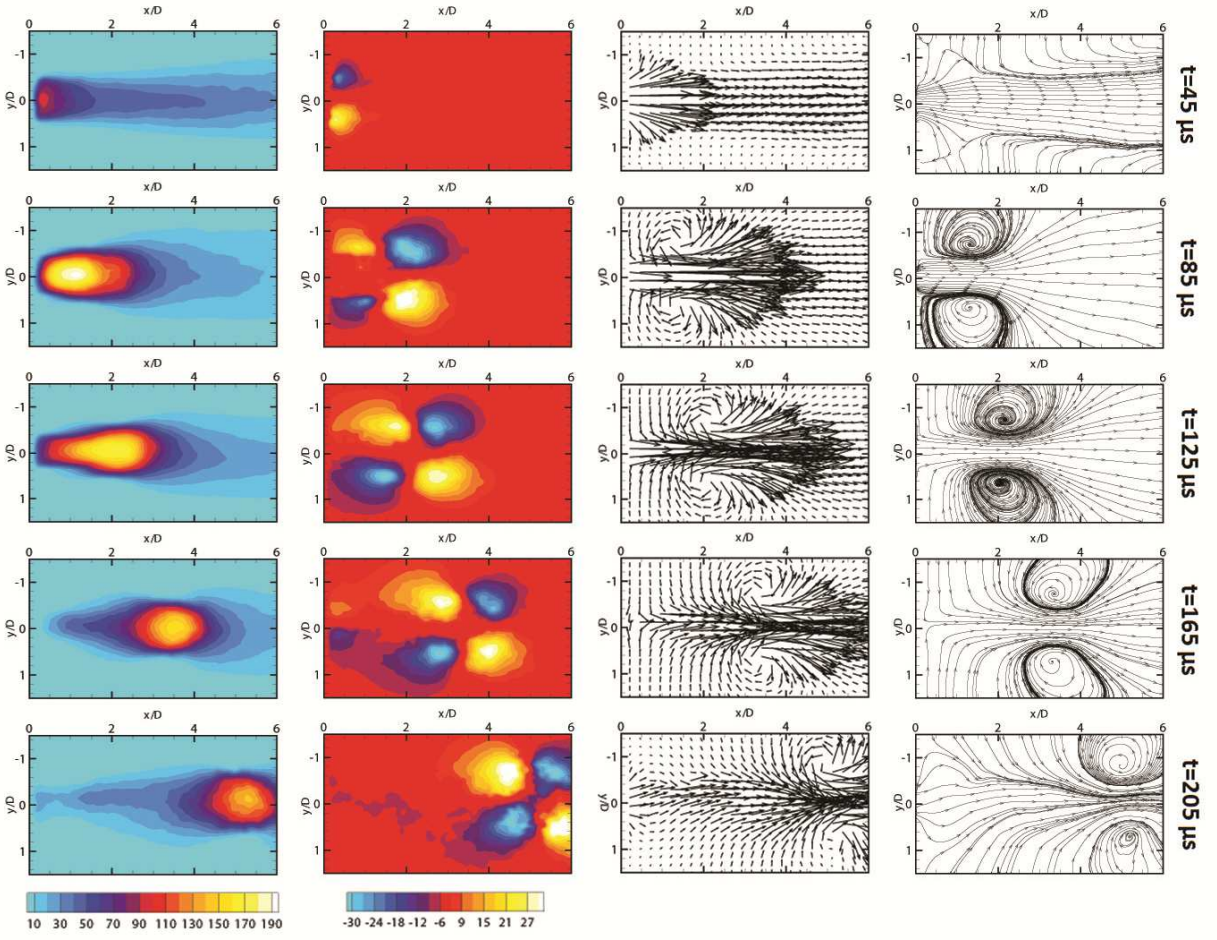

Figure 15: Illustration of the flow field at different phase angle (images are separated by 45 µs) for air pressure of 1.4 bars and volume spark discharge providing energy deposition of 266 mJ per pulse

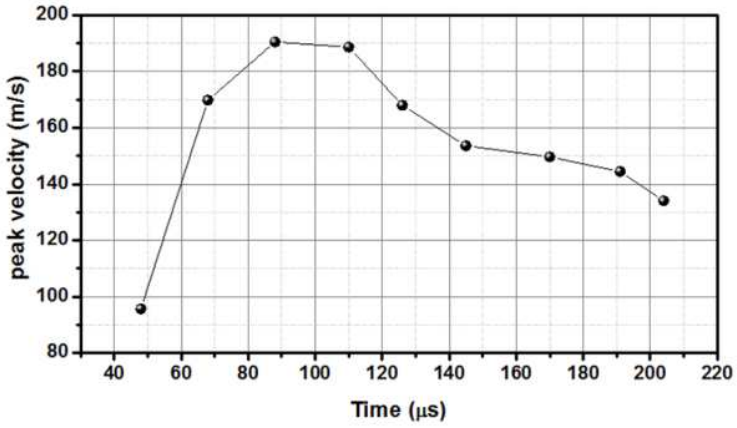

Figure 16: Peak velocity value at different time delays

IV. Conclusion

In addition of the concept description of pulsed jet assisted by plasma, some preliminary results are presented in this study. At this time only results for single pulse plasma are produced. The main electrical characteristics are provided showing that the magnitude of the deposited energy can be varied from 18 to 780 mJ. Semi-qualitative measurements by Schlieren give a first demonstration of the modulation of the output jet topology through the capacitive discharge located in the jet ejection area inside the pressurized chamber. The acceleration of the jet column has been demonstrated qualitatively but also quantitatively by showing that the speed of the front jet can be controlled by the amount of energy deposited in the cavity. The peak velocity has been modulated up to 280%, the jet centerline velocity fluctuating from 50 to 190 $m.s^{-1}$ for a single pulse.

A new series of experiments is actually under progress to characterize the actuator in supersonic configuration and the preliminary results present similar conclusions on the capability of the arc filament to modulate the jet output velocity. These experiments concern the actuator operated in the single pulse mode, but also some tests are initiated to determine the capabilities of the system when trains of pulses are used at different frequencies.

Actually, the actuator is in a preliminary version and a number of aspects have to be improved. The triggering method by a pre-ionization pulse is helpful to guarantee a good timing between the signal command and the ignition of the arc discharge but this is still not perfect as a jitter of about 10 µs is actually observed. The amount of deposited energy has also to be more reliable between two consecutive pulses. A better localization of the arc filament path from the anode to the cathode should be improved. One of the most important actual limitation is the electrode erosion that contributes considerably for reducing the reliability of the actuator, this despite the use of a hard material such as Tungsten. Different approaches are under investigations to solve these issues and an improved design with a reduced size (for easy implementation) should be presented soon.

Acknowledgment

The equipment used in this work was funded by the French Government program “Investissements d’Avenir” (LABEX INTERACTIFS, reference ANR-11-LABX-0017-01) and Région Poitou-Charentes. This work is conducted under DGA supervision and partially funded by ANR (INOPLAS, ANR-13-ASTR-0015-01. N. Benard gratefully thanks Florida State University and FCAAP for the scholar visiting supports in 2018 and 2019 summer periods.

Reference

1. Cattafesta III L.N., Sheplak M., 2011. “Actuators for Active Flow Control”, Annual Rev. Fluid. Mech., Vol. 43: 247-272.
2. Gatski T.B., Bonnet J.P., 2014. “Compressibility, Turbulence and High Speed Flows”, 2nd ed., Elsevier Science Publishing Co Inc, USA.
3. Emerik T, Ali M.Y., Foster C., Alvi F.S., Popkin S., 2014. “SparkJet Characterization in quiescent and supersonic Flow Fields”, Exp Fluids, 55:1858.
4. Gustavsson, P., and Alvi F.S., 2016. “Development and characterization of high frequency resonance-enhanced microjet actuators for control of high speed jets”, Exp Fluids 57-88.
5. Cybyk, B., Grossman, K., and Wilkerson, J., 2004, “Performance characteristics of the sparkjet flow control actuator,” in Proceedings of the 2nd AIAA Flow Control Conference, Portland, OR, USA, 28 June–1 July 2004; p. 2131.
6. Zong, H., Chiatto, M., Kotsonis, M., and De Luca L., 2018, “Plasma synthetic jet actuators for active flow control”, Actuators, Vol. 77.
7. Narayanaswamy, V., Shin, J., Clemens, N., and Raja, L., 2008, “Investigation of plasma-generated jets for supersonic flow control,” In Proceedings of the 46th AIAA Aerospace Sciences Meeting and Exhibit, Reno, NV, USA, 7–10 January 2008; p. 285.
8. Zong, H., and Kotsonis, M., 2017, “Formation, evolution and scaling of plasma synthetic jets,” Journal of Fluid Mechanics, Vol. 837, pp. 147-181.
9. Traldi E., Boselli M., Simoncelli E., Stancampiano A., Gherardi M., Colombo V., and Settles G.S., 2018, “Schlieren imaging: a powerful tool foratmospheric plasma diagnostic,” EPJ Techniques and Instrumentation, Vol. 5
10. Buchmann N.A., Willer C.E., and Soria J., 2012, “Pulsed, high-power LED illumination for tomographic particle image velocimetry,” Exp. in Fluids, Vol. 53.
11. Zong H., and Kotsonis M., 2017, “Effect of slotted exit orifice on performance of plasma synthetic jet actuator,” Exp in Fluids, Vol. 58